European Journal of Chemistry 1 (2) (2010) 96-101

European Journal of Chemistry

Journal homepage: www.eurjchem.com

Optical and gas sensing studies of transparent ZnO thin film deposited from a new precursor by ultrasonic aerosol assisted chemical vapor deposition

Muzammil Hussain[a,*] and Syed Tajammul Hussain[b]

[a] *Department of Chemistry, Quaid-i-Azam University, Islamabad-45320, Pakistan*
[b] *National Centre For Physics, Quaid-i-Azam University Complex, Islamabad-43520, Pakistan*

**Corresponding author at: National Centre For Physics, Quaid-i-Azam University Complex, Islamabad-43520, Pakistan. Tel.: +92.51.2077308; fax: +92.51.2077395.*
E-mail address: dr_tajammul@yahoo.ca (S.T. Hussain).

ARTICLE INFORMATION

Received: 5 March 2010
Received in revised form: 8 April 2010
Accepted: 21 April 2010
Online: 30 June 2010

KEYWORDS

New Precursor
ZnO
Thin Films
CVD
Gas Sensors
Ceramic Substrate

ABSTRACT

Transparent semi-conducting ZnO thin films with low resistivity and high transmittance in the visible optical region were deposited by the decomposition of *bis*(2,4-pentanedionate)-*bis*(aminoethanol) zinc(II) under an atmosphere of oxygen on ceramic, metal and quartz substrates by ultrasonic aerosol assisted chemical vapor deposition. The precursor was synthesized from *bis*(2,4-pentanedionate) zinc(II) and aminoethanol by sonication in acetonitrile and was characterized by melting point, infrared spectroscopy, CHNS-O elemental, atomic absorption, and single crystal X-ray diffraction analysis. TGA-FTIR was used to identify the cause of the weight losses and evolved gases formed during the breakup of the molecules. Electrical and optical measurements showed that the ZnO film has a band gap of 3.02 eV and typical semiconductor properties with a resistivity that depends on the thickness of the film. Powder XRD, SEM and EDX show that films are uniform, smooth and crystalline in nature, giving particle sizes in the range of 30-60 nm and exhibit a (002) orientation with the *c*-axis perpendicular to the substrate surface.

1. Introduction

In the past much attention has been paid to fabricate ZnO thin films with porous microstructure and controlled particle size for technological applications as gas sensors [1], UV light emitters [2], transparent high power electronics [3], piezoelectric transducers [4] and in solar cells [5,6]. The application of ZnO in these devices mainly depends on porosity, particle size and oxygen deficiency of the material deposited. Typically, pure ZnO has a resistivity of 1-100 Ω cm, depending on the deposition technique [7].

Various techniques such as sputtering [8,9], chemical spray deposition [10], sol-gel [11] and electrochemical deposition [12] are available for the deposition of thin films. One of the techniques to deposit thin metal or metal oxide films is Aerosol Assisted Chemical Vapor Deposition (AACVD), which involves the generation of an aerosol using an ultrasonic generator. This technique requires suitable precursors, which can deliver the required metal and metal oxides under controlled reaction conditions to form a high conformal thin film. Particle size, thickness and crystallinity of the deposited films can be controlled by this technique. Most of the precursors used for the deposition of thin films using this technique are metal acetyl acetonates such as $M(acac)_2X_2$ [13-16], $M(acac)_3X$ [17], $M(acac)_4$ [18] and other metal complexes like aminoalkoxides or carboxylates [19,20]. Uses of aminoethanol based precursors give the additional advantage of extra volatility and stability for an extended period of time [21], and these materials have the potential to deliver the required metal or metal oxide to the substrate free of any impurities of carbon in the final oxide film, thus this technique has an advantage over the Sol gel process [22] where the films are of random orientation and contain impurities.

In the present work we report a rapid ultrasonic synthesis of the precursor *bis*(2,4-pentanedionate)-*bis*(2-aminoethanol) zinc(II) and the ultrasonic aerosol assisted deposition of high quality semiconducting thin films with a transmittance of more than 80 % and resistivities of less than 3 Ω cm for application as an antireflective coating.

2. Experimental

2.1. Materials and instrumentation

Analytical grade reagents purchased from Sigma/Aldrich were used for the synthesis of the precursor without further purification and all experiments were performed in air. All other chemicals were purchased from Merck and were used as supplied. All syntheses were performed under ultrasonic irradiation using a 20 KHz ultrasonic generator. Melting points were measured with a GallenKamp 3A-3790 apparatus. Elemental analyses (CHNO & Zn) were performed using a CHNS-O Flash EA 1112 analyzer of Thermoelectron and an Atomic Absorption Analyzer (GBC). Thermal studies and decomposition patterns were studied using a TGA/SDTA 851[e] from Mettler Toledo coupled with an FTIR Nexus 470 of Thermo Nicolet. The molecular structure of *bis*(2,4-pentanedionate)(aminoethanol) zinc(II) was determined using a Bruker AXS SMART APEX CCD diffractometer at 100(2) K with monochromatic Mo Kα radiation and the omega scan technique. The unit cell was determined using SAINT+ [23] and the data were corrected for absorption using SADABS in SAINT+ [24]. The structure was solved by direct methods and

ISSN 2153-2249 (Print) / ISSN 2153-2257 (Online)
DOI:10.5155/eurjchem.1.2.96-101.49

refined by full matrix least squares against F^2 with all reflections using SHELXTL [25]. Refinement of an extinction coefficient was found to be insignificant. All non-hydrogen atoms were refined anisotropically. Film thicknesses were measured using a sigma scan analyzer (Stylo, USA). The deposited thin film thickness comes out in the range of 75 nm-80 nm. Powder X-ray diffraction studies were performed using a PAN Analytical X' Pert PRO diffractometer equipped with a Cu source (Cu K_α, λ = 1.5405 Å). Peak intensities, d-spacing, 2θ values and integral breadth of the reflections were determined with X'Pert Data Collector software. Thin film surface morphology, average particle size and composition of the deposited material were observed by SEM and EDX (JOEL-JSM-5910). The optical transmittance of the ZnO films was determined using a UV-Vis spectrophotometer (MPC-3100, Schimadzu). The electrical properties of the oxide films under various conditions were measured by an in house developed two probe set up as previously reported [26].

2.2. Synthesis of bis(2,4-pentanedionate) Zinc(II)

In a 250 mL Erlenmeyer flask containing 10 mL of distilled water, 0.3 g (1.67 mmol) of $ZnSO_4.H_2O$ were added. The solution was irradiated in an ultrasonic generator to dissolve the salt. An ammoniacal solution of 2,4-pentanedionate (acac) prepared by mixing 0.33 g (3.3 mmol) of acetylacetone, 4 mL of distilled water and 0.8 mL of a 5 M ammonia solution was added drop wise to a zinc sulfate solution under constant ultrasonic irradiation. The mixture was further irradiated for about 30 minutes. A solid mass that separated out on cooling was filtered and washed with diethyl ether, dried under vacuum and recrystallized from methanol to yield white needles, m.p. 158 °C in 80% yield. The CHNO analysis % found (calculated) for $C_{10}H_{14}O_4Zn$ is C 45.37 (45.8), H 5.40 (5.34), O 24.38 (24.4), the atomic absorption spectroscopy analysis % found (calculated) is Zn 24.51 (24.42).

2.3. Synthesis of bis(2,4-pentanedionate)-bis(amino ethanol)zinc(II)

In a 250 mL Erlenmeyer flask, 2.6 g (10 mmol) of $Zn(acac)_2$, 1.6 g (20 mmol) of 2-aminoethanol (ea) and 30 mL of acetonitrile were mixed. The flask was covered with a polythene film and then placed in an ultrasonic generator at a temperature of 40 °C for 5-6 min to produce a clear solution. The contents were taken out of the ultrasonic bath and set aside at room temperature for crystallization. White needles of *bis*(2,4-pentanedionate)-*bis*(aminoethanol)zinc(II) were obtained (M.p. 140 °C) in 90 % yield, were filtered, washed with petroleum ether and dried in air. The CHNO analysis, % found/calculated for $C_{14}H_{28}O_6N_2$ Zn is C 42.7 (43.63), H 7.11 (7.2), O 24.1 (24.88), N 7.35 (7.2), the atomic absorption spectroscopy analysis % found/calculated for $C_{14}H_{28}O_6N_2Zn$ is Zn 16.78 (16.85). FTIR (cm^{-1}): 3318, 3268, 2940, 2880, 1580, 1509, 1397, 1351, 1308, 1245, 1197, 1144, 1245, 1197, 1116, 1073, 1052, 917, 865, 849, 770, 650.

2.4. Thermal studies

Thermal behavior of $Zn(acac)_2(ea)_2$ was studied in the range of 30–500 °C with a heating rate of 10°C/min under an O_2 atmosphere in an open lid 70 µL alumina crucible using a Mettler Toledo TGA/SDTA 851^e instrument to determine the decomposition temperature. The purge gas and the evolved gases from the sample were transferred from the TGA to the FTIR through a transfer line that was kept constantly at 250°C in order to avoid any condensation of the evolved gases. FTIR scans of the gases were taken at *ca*. every twenty seconds at a resolution of 4 cm^{-1}.

2.5. Thin film deposition

The thin film deposition apparatus was described previously in detail [26]. The conditions used for the growth of the ZnO thin films are given in Table 1. A solution of 200 mg/25 mL in methanol was injected into an Ultrasonic Atomizer (Cole Palmer) to generate the aerosol in an evacuated quartz chamber containing 50×40 mm gold coated ceramic wafers. The ceramic wafer was cleaned with deionized water, acetone and 1,1,1-trichloro ethane and then heated to 100 °C for twenty minutes before use. Oxygen and sample solution was injected through a control valve.

Table 1. Growth condition for the deposition of metal oxide thin film from *bis*(2,4-pentanedionate)-*bis*(aminoethanol)zinc(II).

Precursor concentration	200 mg/25 mL (Methanol)
Carrier Gas (O_2) flow rate (cm^3/min)	25
Sample solution injection (mL/min)	0.5
Substrate	Quartz, Ceramic, Stainless steel.
Deposition time	0-30 min (depending on thickness)

3. Results and Discussion

Bis(2,4-pentanedionate)zinc(II) [$Zn(acac)_2$] dissolved in acetonitrile reacts quantitatively with 2-aminoethanol (ea) under ultrasonic irradiation to give $Zn(acac)_2$ $(OHC_2H_4NH_2)_2$ m.p. 140 °C in 90 % yield.

$$Zn(acac)_2 + 2OHC_2H_4NH_2 \xrightarrow[\text{acetonitrile}]{\text{Ultrasonic irradiation}} Zn(acac)_2(OHC_2H_4NH_2)_2$$

The characteristic I.R vibrational frequencies are found in agreement with the proposed structure. N-H and OH stretching frequencies were found at 3400-3268 cm^{-1} and 3318 cm^{-1}, respectively. N-H out-of-plane bending at 849-770 cm^{-1} and C-N stretching at 1197-1116 cm^{-1} indicate the presence of 2-aminoethanol. Carbonyl stretching absorption bands of acac ligands are at 1580 cm^{-1}. Bands at 917 cm^{-1} and 650 cm^{-1} are due to the vibration of M-N and M-O bonds, respectively.

3.1. Single crystal X-ray analysis

The single-crystal X-ray analysis confirms the spectroscopic data. The molecular structure of *bis*(2,4-pentanedionate)-*bis*(2-aminoethanol) zinc(II), is shown in Figure 1. Thermal ellipsoids are drawn at the 50% level, hydrogen atom spheres are at arbitrary radii. Only the major disordered moieties are shown. The structure shows two types of disorders: The alcohol oxygen atom and the acac ligand are each disordered over two positions. The occupancy ratios are 0.526(4) to 0.474(4) for the OH group and 1:1 (unrefined) for the acac anions. The acac carbon atoms of each moiety were restrained to be flat within a standard deviation of 0.1, carbon atoms C2 and C4 were restrained to be isotropic within standard deviation of 0.001, and all disordered carbon atoms were restrained to have same anisotropic displacement parameters as their disordered counterparts. All hydrogen atoms were placed in calculated positions and were refined with an isotropic displacement parameter of 1.5 (methyl, hydroxyl) or 1.2 times (all others) that of the adjacent carbon or oxygen atom. The zinc ion has a distorted octahedral geometry surrounded by two acac anions acting as bidentate O-donor ligands and two monodentate aminoethanol ligands coordinating via the N atoms in trans position to each other. A summary of the crystallographic data and refinement parameters for $Zn(acac)_2$ $(OHC_2H_4NH_2)_2$ are given in Table 2 and selected bond lengths and angles are recorded in Table 3. All hydrogen bonds were tabulated in Table 4. All hydrogen atoms were placed in calculated positions and were refined with an anisotropic displacement parameter of 1.5 (methyl, hydroxyl) or 1.2 times (all others) that of the adjacent carbon or oxygen atom.

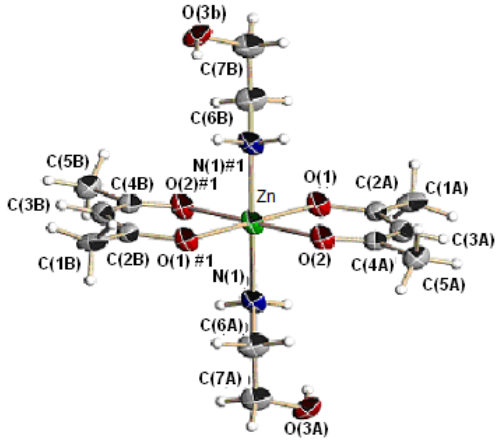

Figure 1. Crystal structure of *bis*(2,4-pentanedionate)-*bis*(aminoethanol) zinc(II), $Zn(acac)_2$ $(OHC_2H_4NH_2)_2$.

Table 2. Crystal data for *bis*(2,4-pentanedionate)-*bis*(aminoethanol)zinc(II), $Zn(acac)_2$ $(OHC_2H_4NH_2)_2$.

Molecular formula	$C_{14}H_{28}N_2O_6Zn$
Formula weight	385.75
Temperature	100K
Crystal system	Triclinic
Space group	P-1
Unit Cell Dimensions	a=5.3009(7) Å
	b=9.3724(12) Å
	c=9.5074(12) Å
	α=73.149(2)°
	β=83.479(2)°
	γ=76.561(2)°
Volume, Z:	439.15(10) Å^3, 1
Density (calculated)	1.451 Mg/m^3
Absorption coefficient	1.428 mm^{-1}
F(000)	202
Crystal size	0.50 × 0.05 × 0.02 mm
Crystal shape, color	rod, colorless
θ range for data collection	2.24 to 28.28°
Independent reflections	2159 (R_{int} = 0.023)
Reflection collected	4554
Refinement method	Full-matrix least square on F^2
Final R indices [$I>2\sigma(I)$]	R1 = 0.0357, wR2 = 0.0866
R indices (all data)	R1=0.0382, wR2 = 0.0884

Table 3. Some important bond lengths [Å] and angles [°] for **(**$Zn(acac)_2$ $(OHC_2H_4NH_2)_2$**)**

Bond Lengths (A°)		Bond Angles. (°)	
C(1A)-C(2A)	1.503(9)	O(1)-C(2A)-C(3A)	125.4(6)
C(2A)-O(1)	1.215(7)	O(1)-C(2A)-C(1A)	117.2(5)
C(2A)-C(3A)	1.416(8)	C(3A)-C(2A)-C(1A)	117.4(5)
C(3A)-C(4A)	1.352(9)	C(4A)-C(3A)-C(2A)	129.2(6)
C(4A)-O(2)	1.321(6)	O(2)-C(4A)-C(5A)	113.4(6)
C(1B)-C(2B)	1.537(9)	C(3A)-C(4A)-C(5A)	121.9(6)
C(2B)-O(1)	1.263(6)	N(1)-C(6)-C(7A)	113.05(18)
C(2B)-C(3B)	1.398(8)	C(6)-N(1)-Zn(1)	120.20(14)
C(3B)-C(4B)	1.464(9)	C(2A)-O(1)-Zn(1)	127.1(3)
C(4B)-O(2)	1.155(6)	O(3A)-C(7A)-C(6)	115.5(2)
C(4B)-C(5C)	1.519(10)	O(2)#1-Zn(1)-O(2)	180.0
C(6)-C(7A)	1.512(3)	O(2)#1-Zn(1)-O(1)#1	87.55(6)
N(1)-Zn(1)	2.1270(19)	O(2)#1-Zn(1)-N(1)	92.07(6)
O(1)-Zn(1)	2.1199(15)	O(1)-Zn(1)-N(1)	91.54(7)
O(2)-Zn(1)	2.1097(14)	O(2)#1-Zn(1)-N(1)#1	87.93(6)
C(7A)-O(3A)	1.374(4)	O(2)-Zn(1)-N(1)#1	92.07(6)
Zn(1)-O(2)#1	2.1097(14)	N(1)-Zn(1)-N(1)#1	180
Zn(1)-O(1)#1	2.1199(15)		
Zn(1)-N(1)#1	2.1270(19)		

Symmetry transformations used to generate equivalent atoms: #1 -x+2,-y+2,-z

Table 4. Hydrogen bonds for **(**$Zn(acac)_2(OHC_2H_4NH_2)_2$**)** [Å and °].

D-H...A	d(D-H)	d(H...A)	d(D...A)	<(DHA)
O(3B)-H(4)...O(2)#2	0.84	2.02	2.831(4)	161.1
O(3A)-H(3C)...O(1)#3	0.84	2.07	2.902(3)	168.6
N(1)-H(1H)...O(1)#3	0.92	2.35	3.136(2)	143.6
N(1)-H(1G)...O(2)#2	0.92	2.31	3.127(2)	147.3

Symmetry transformations used to generate equivalent atoms: #1: -x+2, -y+2, -z; #2: -x+1, -y+2, -z; #3: x-1, y, z.

3.2. Thermal studies

TGA and DTG curves for the decomposition of *bis*(2,4-pentanedionate)-*bis*(aminoethanol)zinc (II) were recorded in an oxygen environment and are shown in Figure 2. The TG curve of the complex shows a three step weight loss at temperatures ranging around 100 - 210, 210 - 260 and 260 - 400 °C to give a residual value close to that expected for a complete conversion to zinc oxide and volatile by-products. The DTG curve shows three prominent exothermic peaks. The peak around 200 °C is assigned to the release of aminoethanol which yielded a weight loss of 32 %. This is in good agreement with the theoretical stoichiometric value of 31.6 % for amino ethanol. The second and third exothermic peaks at 240 and 370 °C are assigned to the weight loss due to acetylacetone ligands breaking up and being lost as volatile material to leave 21% of ZnO as the final residue.

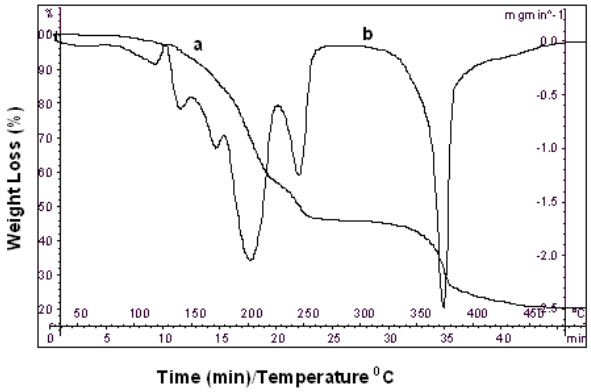

Figure 2. TGA/DTG curves showing the decomposition of *bis*(2,4-pentan edionate)-*bis*-(aminoethanol)zinc(II).

3.3. Thermo gravimetric analysis (TGA)-FTIR studies

The thermal decomposition pattern of *bis*(2,4-pentanedionate)-*bis*(aminoethanol)zinc(II) is shown in Scheme 1. The pattern is in line with the infrared data of the evolved gaseous products taken at various time intervals/temperatures as shown in Figure 3.

$$Zn(acac)_2(ea)_2 \xrightarrow[O_2]{200\ ^oC} Zn(acac)_2 + 2ea$$

ea = $H_2NC_2H_4OH$, acac = $C_5H_7O_2$

$$Zn(acac)_2 \xrightarrow[6O_2]{260\ ^oC} acacH + 2CO_2 + CH_3COCH_3 + ZnO$$

$$3acacH \xrightarrow[2O_2]{>300\ ^oC} 4CH_3COCH_3 + 3CO_2$$

Scheme 1

Studying Figure 3, it is reasonable to believe that the aminoethanol ligand is lost first. This is supported by the evolved gas IR spectrum below a temperature of 200 °C which shows prominent peaks for free OH, NH_2 and C-H groups at 3650-3600 cm^{-1}, 3400-3268 cm^{-1} and 3000-2850 cm^{-1}, respectively (Spectrum c), and also by the FTIR spectrum of the residue of the TGA studies at 200°C which clearly shows the absence of prominent aminoethanol peaks (Spectrum b). In the second stage above 200 °C the weight loss was due to one of the acac anions leaving as acacH, as confirmed by the evolved gas spectrum (d). The acacH is probably formed by abstraction of a proton from the remaining ligand, which ultimately at higher temperature in the atmosphere of oxygen seems to be reacting with oxygen to form the volatile compounds acetone and CO_2 with distinct bands of 1220, 1360, and 1740 cm^{-1} spectrum (e) leaving pure ZnO as the residue.

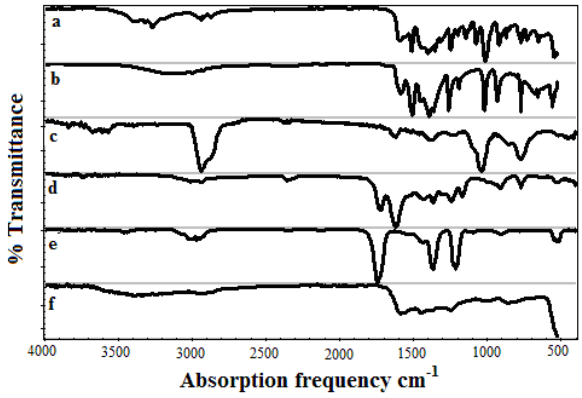

Figure 3. Linked spectra of TGA-FTIR: a) FTIR spectrum of *bis*(2,4-pentanedionate)-*bis*(aminoethanol)zinc(II) at room temperature, b) FTIR spectrum of *bis*(2,4-pentanedionate)-*bis*(aminoethanol)zinc(II) after heating to 200 °C, c) evolved gas spectrum below 200 °C (mainly aminoethanol) d) evolved gas spectrum at 250 °C, (mainly acacH) e) evolved gas spectrum above 300 °C (mainly acetone), f) evolved gas spectrum at > 350 °C.

Based on the FTIR studies and previous [27] work we suggest the following pyrolysis mechanism (Scheme 1) for the decomposition of *bis*(2,4-pentanedionate)-*bis*(aminoethanol) zinc(II) to zinc oxide.

These findings are contrary to a previous study [28,29] in which the amine group facilitated the cleavage reaction of the acetylacetone ligand by the removal of CO_2. In the present study after the loss of aminoethanol in the first stage the acac group attached to zinc metal follow the above suggested cleavage mechanism at high temperature.

3.4. Scanning electron microscopy (SEM) and electron dispersion X-ray (EDX) studies

Figure 4 shows a scanning electron microscopy image of the deposited ZnO particles. The SEM micrograph indicates uniform deposition of ZnO nano particles with sizes ranging from 30 nm to 60 nm. EDX analysis (Figure 5) confirms that the film comprises of pure zinc oxide particles.

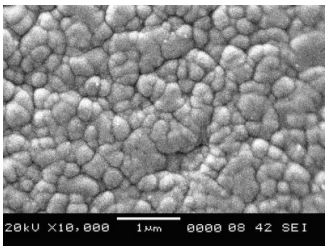

Figure 4. Scanning Electron micrograph of ZnO deposited from *bis*(2,4-pentanedionate)-*bis*(ethanolamine)zinc(II).

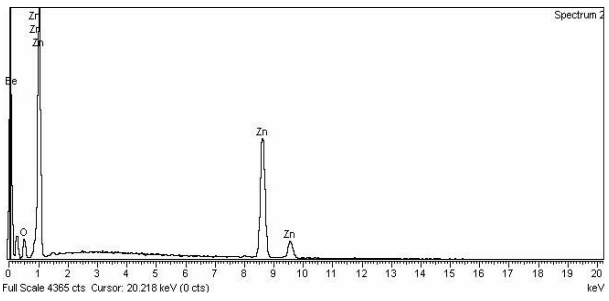

Figure 5. EDX Analysis of ZnO film.

3.5. X-ray diffraction (XRD) studies

The XRD pattern of a ZnO film within an angle range of 15 to 80° is shown in Figure 6. The ZnO has been found to exist in hexagonal wurtzite form (space group $P6_3mc$, a = 3.186, c = 5.206, JCPDS standard data PDF # 050644). The pronounced (002) peak located at 2θ = 34.41 indicates a preferential orientation along the c-axis perpendicular to the substrate surface as reported earlier [9].

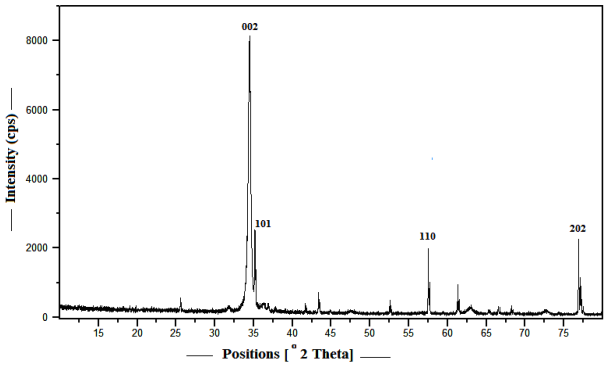

Figure 6. XRD pattern of Zinc Oxide Film on Ceramic Substrates.

The ultrasonic aerosol assisted chemical vapour deposition technique has an edge over the ultrasonic irradiation assisted solution route [30], which was based on traditional precipitation theory and involves multiple deposition cycles. Typically 20 deposition cycles were performed before ultrasonic irradiation of substrates. The high velocity microjets produced during ultrasonic irradiation remove the large & loosely bonded particles and significant reduction in the quantity of adsorbed particles may account for the enhaced crystallinity and preferential orientation along (002) plane. Where as in our case ultra fine droplet of precursor having narrow size distribution in range of a few micrometers comes in contact with hot substrate and decomposes to highly uniform spot free film with enhanced crystallinity and preferential (002) plane of pure zinc oxide in oxygen environment.

The particle size was calculated using the Scherrer equation t = Kλ/B cos θ, with t being the averaged dimension of the crystallites, K the Scherrer constant (a somewhat arbitrary constant in the range 0.87-1); λ is the wavelength of X-rays; and B is the integral breadth of a reflection (in radians 2θ) located at 2θ. B for the (002) peak found here is 0.2362° rad. (θ = 17.205°, λ =1.5405 Å). Assuming K to be 0.9, results in a value for the averaged crystal size of 35 nm, which is in good agreement with the values of 30-60 nm measured by SEM.

3.6. Optical and sensing studies

The optical transparency depends on operating temperature, deposition conditions and oxidation processes during the growth of ZnO thin film. Figure 7 shows the optical transmission spectrum of the (002) oriented ZnO thin film in the wavelength range of 300 to 800 nm.

The wide band gap in these films give high transmittance above 600 nm with an absorption edge around 372 nm as reported in literature [12]. The optical band gap of the film was calculated from the plot of hν (ev) vs $(\alpha\, t.\, h\nu)^2$ $(ev)^2$ as shown in Figure 8, where t is thickness, hν is the energy of incident light and α is absorption coefficient. The value of band gap thus calculated falls at 3.02 eV which is in good agreement with the reported value of 3.27 eV [31].

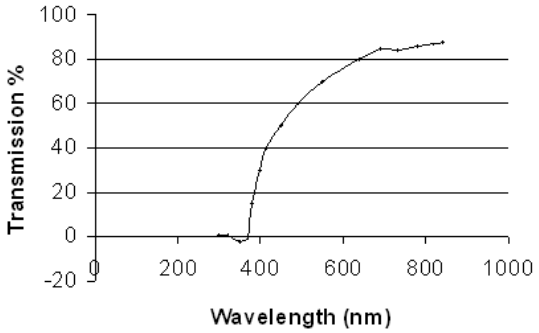

Figure 7. Optical transmittance of ZnO film on fused silica quartz.

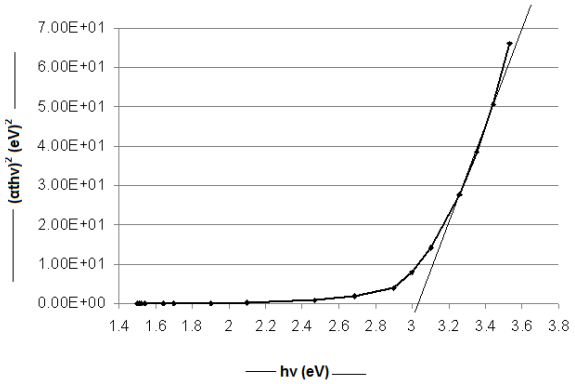

Figure 8. Absorption coefficient (α) vs photon energy (hν) curve of ZnO thin film.

Electrical conductivity in the semiconducting metal oxide is due to non-stoichiometric composition as a result of oxygen deficiency and the electron concentration near the surface [32]. Moreover, the operating temperature has also profound effect on the mechanism of desorption and decomposition of a test gas to achieve the maximum sensitivity. In the present study the change in the electrical resistance of a sensor for a natural gas (methane) was measured by the experimental arrangements mentioned elsewhere [26].

In case of Natural Gas (Methane) sensing, ZnO thin film gas sensor when exposed to natural gas fed in to gas sensing measuring device through a gas flow controller causes a appreciable change in the resistance at a temperature of 200 °C. The maximum response was observed at a temperature of 200 °C, however, at low temperature not only its response time increases but also its sensitivity decreases manyfolds. A plot of the operating temperatures and sensitivity for 500 and 1000 ppm natural gas is presented in Figure 9.

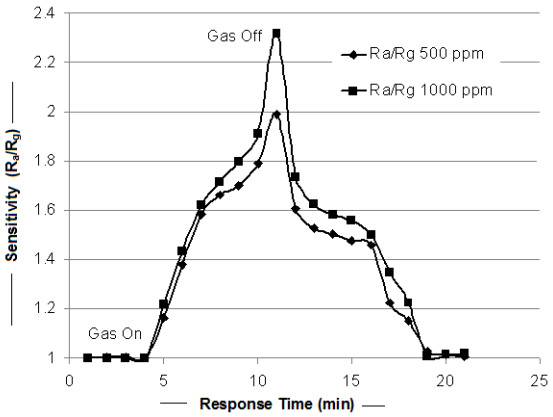

Figure 9. Sensor Response Time of Film in Natural gas (Methane) environment.

The gas sensing mechanism in case of methane gas sensor, supposing that the environmental oxygen (O_2) adsorbed on the surface as O_2^- or O^- by removing the electron density from the conduction band, is developing a depletion region on the surface. The reaction kinematics will be as follows;

$$O_2 \text{ (gas)} \leftrightarrow O_2 \text{ (adsorbed)}$$
$$O_2 \text{ (adsorbed)} + e^- \rightarrow O_2^-$$
$$O_2^- + e^- \rightarrow 2\,O^-$$

When methane gas molecule come in contact with this adsorbed oxygen, leading to an inverse charge transfer upon the return of electron to the conduction bands [33]. The depletion region created by the chemisorptions of O_2 on the surface now filled by electrons and thus resistance change was observed and increase in the height of the conduction bands or conductivity takes place. The possibility of a reaction of methane gas with ZnO thin film can be explained as follows;

$$CH_4 + 4[O^-] \rightarrow CO_2 + 2H_2O + 4e^-$$

The sensitivity regarding the response time in our case is much lower (5 min.) than the previous study (40 min.) [34], where antimony oxide (Sb_2O_3) was used for the detection of methane gas.

4. Conclusions

Ultrafine and transparent ZnO thin films with particle sizes ranging from 30-60 nm can be deposited from *bis*(2,4-pentanedionate)-*bis*(aminoethanol)zinc(II) by ultrasonic aerosol assisted chemical vapour deposition on quartz and ceramic substrate. ZnO seems to be a promising semiconducting material for the detection of oxygen and other reduced gases. The electrical and optical measurements of the thin film demonstrate its suitability for its use as gas sensors, antireflection coatings and in solar cells. Studies by TGA-FTIR allowed elucidating a potential decomposition pattern pathway.

Acknowledgement

The authors are thankful to the Higher Education Commission, Pakistan for financial support.

References

[1]. Sberveglieri, G. *Sens. Actuators. B.***1995,** *23,* 103-109.
[2]. Chang S. J.; SuY. K.; Shei Y. P. *J. Vac. Sci. Technol. A* **1995,** *13,* 385-388.
[3]. Gopel W. *Sens. Actuators. B.* **1994,** *18,* 1-21.
[4]. Magar S.; Kumar S.; Bhatnagar M. *Appl. Phys. Lett.* **1986,** *49,* 394-400.
[5]. Beek W. J. E.; Wienk M. M.; Janssen R. A. J. *Adv. Funct. Mater.* **2006,** *16,* 1112-1116.
[6]. Ma J.; Ji F; Ma H.; Li S. *Solar Energy Materials and Solar Cells*, **2000,** *60,* 341-348.
[7]. Ellmer K. *J. Phys. D: Appl. Phys.* **2000,** *33,* R17-R32.
[8]. Patil1 R. S.; Pathan H. M.; Gujar T. P.; Lokhande D.; Jayaraj M. K.; Antony A.; Ramachandran M. *J. Mater. Sci.* **2006,** *41,* 5723-5725.
[9]. Czternastek H. *Opto-Electron. Rev.* **2004,** *12,* 49–52.
[10]. Natsume Y.; Sakata H. *J. Mater. Sci. Mater. Electron.* **2001,** *12,* 87-92.
[11]. Cammarata R. C. *Scr. Mater.* **2004,** *50,* 751-755.
[12]. Zhao W. B.; Zhang X. D.; Ye Z. Y.; Zhang J. L.; Li C. Y.; Yin D. L.; Gu Z. N.; Zhou X. H.; Jin Z. X. *Thin Solid Films*, **1994,** *240,* 14-21.
[13]. Dahl G. H.; Block B. P. *Inorg. Chem.* **1966,** *5,* 1394-1396.
[14]. Harrod J. F.; Taylor K. R. *Inorg. Chem.* **1975,** *14,* 1541-1545.
[15]. Bickley D. G.; Serpone N. *Inorg. Chem.* **1979,** *18,* 2200-2204.
[16]. Schmidke H. H.; Voets U. *Inorg. Chem.* **1981,** *20,* 2766-2771.
[17]. Lin C.; Kagan C. R. J. Am. Chem. Soc. **2003,** *93,* 336-337.
[18]. Chun H. K.; Steffen W. L.; Fay R. C. Inorg. Chem. **1979,** *18,* 2458-2465.
[19]. Pinnavaia T. J.; Mocella M. T.; Averill B. A.; Woodard J. T. *Inorg Chem.* **1973,** *12,* 763-768.
[20]. Manzer L. E. *Inorg. Chem.* **1978,** *17,* 1552–1558.
[21]. Srinivasan G.; Kumar J. *Cryst. Res.Tech.* **2006,** *41,* 893-896.
[22]. Zhang C. *J. Phys. Chem. Solids.* **2010,** *71,* 364-369.

[23]. Amiri M. G.; Morsali A.; Hunter A. D.; Zeller M. *Solid state Sci.* **2007,** *9,* 1079-1084.
[24]. Zeller M.; Hunter A. D.; McCarthy J. R.; Capetta S. H.; Bruckner C. *J. Chem. Crystallg.* **2005,** *35,* 935-942.
[25]. Sheldrick G. M. SHELXL-97, Program for Crystal Structure Refinement, University of Göttingen, **1997.**
[26]. Mazhar M.; Hussain S.M.; Rabbani F.; Kociok-Köhn G.; Molloy K. C. *Bull. Korean Chem. Soc.* **2006,** *27,* 1572-1576.
[27]. Yi F.; Ye F.; William G. S.; Collinson M. *J. Phys. Chem.* **2006,** *110,* 9164-9170.
[28]. Gasgnier M. *Adv. Mater.* **1986,** *114,* 11-16.
[29]. Romeo A.; Terheggen M.; Abou-Ras D.; Bätzner D. L.; Haug F. J.; Kälin M.; Rudmann D.; Tiwari A. N. *Adv. Mater.* **2004,** *12,* 93-111.
[30]. Gao X. D., Li X. M.; Yu W. D., *Thin Solid Film.* **2005,** *484,* 160-164.
[31]. Gomos C.; Ozkendir O. M.; Kavak H.; Ufuktepe Y. J. Optoelectron. Adv. Mat. **2006,** *8,* 299-305.
[32]. Chou S. M.; Teoh L. G.; Lai W. H.; Su Y. H.; Hon, M. H. *Sens.* **2006,** *6,* 1420-1427.
[33]. Shiyoshi Y.; Ayumi Y.; Tomoka U.; Masayoshi W.; Kohei S.; *Chem. Lett.* **1990,** *19,* 779-782.
[34]. Tsutsumi N.; Sakata K; Kunitake T. *Chem. Lett.* **1992,** *21,* 1465-1468.